Chemisorption of Acetone on Carbon Nanotubes

Nirupama Chakrapani,*,† Yiming M. Zhang,‡ Saroj K. Nayak,‡ James A. Moore,§ David L. Carroll,|| Yoon Y. Choi,† and Pulickel M. Ajayan†

Department of Material Science and Engineering, Department of Physics, Applied Physics and Astronomy, and Department of Chemistry, Rensselaer Polytechnic Institute, Troy, New York 12180, and Department of Physics and Astronomy, Clemson University, Clemson, South Carolina 29634

Received: April 10, 2003; In Final Form: June 14, 2003

Temperature-programmed desorption experiments show that acetone chemisorbs on nanotubes while physisorption occurs on graphite. Computed high binding energies for chemisorption using hybrid quantum mechanical and semiempirical calculations are in good agreement with the experimental thermal desorption data. The strong chemical interactions between acetone and the nanotube surface are established as being due to the effects of curvature and topological defects.

1. Introduction

Adsorption of simple gas molecules such as helium, methane, and oxygen on nanotubes[1−5] have been studied extensively, though solvent adsorption needs further study. This could have an impact in separations technology[6] using nanotube membranes and also in surface modification of nanotubes by straightforward methods. Credence to this is given by studies wherein carbon nanotubes have been found to react with some solvents such as monoclorobenzene[7] and aniline[8] on sonication or refluxing. Most methods of nanotube processing involve use of solvents and sonication which could affect both the surface properties as well as the structure of nanotubes. Adsorption of acetone on graphite[9,10] has been studied quite extensively as graphite is a standard substrate for investigations on 2D adsorbed phases.[11,12] A study of the difference in adsorbate properties of solvent molecules on nanotubes and graphite could also help us to understand the dependence of adsorption on surface curvature. In this paper, we report studies on adsorption of acetone on carbon nanotubes both by experimental methods and hybrid quantum mechanical and semiempirical calculations. It is observed that acetone strongly chemisorbs on nanotubes and remains stable until high temperatures, unlike its behavior on graphite, and this adsorption phenomenon is common to both single- and multi-walled nanotubes.

2. Experimental Details

The single-walled nanotubes (SWNT) produced by the HiPCO[13] process were used without further purification. The acetone-adsorbed nanotubes (s-SWNT) samples were prepared by ultrasonication (Sonics, Vibra-Cell) of 10 mg of nanotubes in 300 mL of acetone (Fisher GC resolve) for 1 h. The solvent was allowed to evaporate naturally. These air-dried, ultrasonicated samples (s-SWNT) were used in all the experiments. X-ray photoelectron spectroscopy (XPS) was done using Mg Kα line in ultrahigh vacuum ($<10^{-10}$ Torr) on acetone-treated nanotubes to determine the percentage of oxygen on the surface and its binding energy. Tempertaure-programmed desorption (TPD) was performed using an SRS Residual Gas Analyzer to study the desorption kinetics of acetone from s-SWNT and pristine single-walled nanotubes (p-SWNT) to study desorption kinetics. The TPD experiments were carried out in a high-vacuum chamber that was first purged with argon and then pumped down to 10^{-8} Torr. A heating rate of 3 °C per minute was used to heat the sample from room temperature to 700 °C. The partial pressure and atomic mass of the different species that desorbed at different temperatures was obtained. The identification and peak assignments were made on the basis of the fragmentation pattern of acetone in mass spectroscopy. A plot of partial pressure against temperature of a particular species gave the desorption characters of that species. The acetone-treated single-walled nanotubes were also characterized by micro-Raman spectroscopy using a GRAMS/32 spectral notebase working with a 514.5 nm argon ion laser.

3. Results and Discussion

XPS was performed on s-SWNT and p-SWNT for surface chemical analysis. As a control, nanotubes stirred in acetone (without ultrasonication) for 1 h were also used. The C1s and O1s peaks were scanned in high resolution. The pristine nanotubes showed a presence of 1% (atomic) oxygen relative to carbon. An increase in oxygen concentration (5%) was observed in s-SWNT, though not much increase was seen in nanotubes stirred in acetone, possibly due to exposure of very low surface area to acetone. The oxygen 1s peak of the acetone sonicated sample was resolved into two Gaussian peaks (Figure 1) one at 532.2 eV and the other at 529.7 eV. The two different binding energies of oxygen suggest two different bond structures for adsorbed oxygen.[14] Acetone is known to dissociate on chemisorption[14] on the Si(100) surface with partial and complete carbonyl bond cleavage, the evidence for which was seen in XPS and TPD. As the percentage of adsorbed acetone was less, no appreciable change was observed in the C1s peak position centered at 284.5 eV, though the intensity of the high energy tail increased, which represents the sp^3 carbon.

The thermal desorption spectra of acetone was obtained by monitoring the 43 (CH_3CO), 58 (CH_3COCH_3), and 15 (CH_3)

* Corresponding author. E-mail: chakrn@rpi.edu.
† Department of Material Science and Engineering, Rensselaer Polytechnic Institute.
‡ Department of Physics, Rensselaer Polytechnic Institute.
§ Department of Chemistry, Rensselaer Polytechnic Institute.
|| Department of Physics and Astronomy, Clemson University.

10.1021/jp034970v CCC: $25.00
Published on Web 08/02/2003

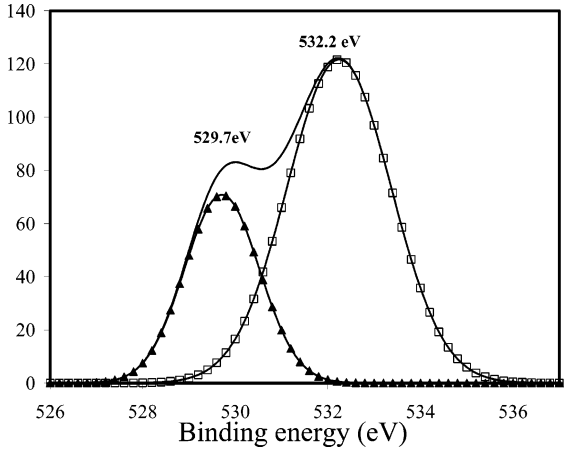

Figure 1. Oxygen 1s spectra of acetone-treated carbon single-walled nanotubes from XPS. The deconvoluted spectrum shows the presence of two peaks at 529 eV and 532 eV.

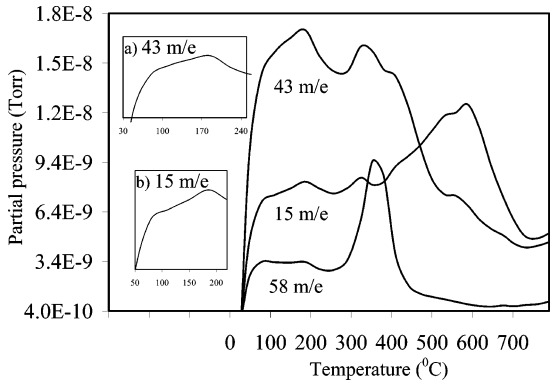

Figure 2. Thermal desorption profile of $m/e = 58$ (CH_3COCH_3), 43 (CH_3CO), and 15 (CH_3), which correspond to different fragments of acetone. The appearance of the desorption peak at 78 °C can be seen clearly in insets (a) and (b).

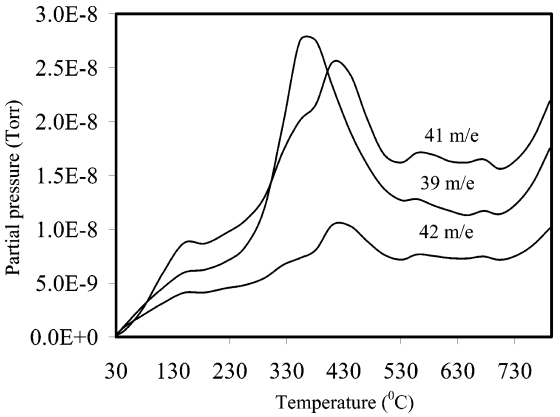

Figure 3. The thermal desorption traces of $m/e = 41$, 39, and 42. These mass units correspond to the fragmentation pattern of propylene in mass spectroscopy.

m/e (Figure 2) signals which correspond to the fragmentation pattern of acetone in mass spectroscopy.[15,16] The observed peak temperatures for $m/e = 43$ and 15 were 78 °C, 186 °C, 353 °C, 441 °C, and 558 °C. The first three peaks were also seen in the 58 *m/e* signal. Apart from that, very strong signals of *m/e* values of 41, 39, and 42 (Figure 3) were observed in the temperature range of 350−450 °C, and these signals correspond to the fragmentation pattern of propylene.[15,16] We found that their peak positions were similar, indicating that they are fragments of the same species. Desorption of propylene, which would result from the adsorbed alkyl (CH_3-C-CH_3) fragments of acetone, further confirms chemisorption. As both propylene and acetone signals were seen at high temperatures (441 °C and 558 °C), probably two different types of chemisorption occurred. At 353 °C, two peaks corresponding to $m/e = 115$ and $m/e = 116$ were observed. Surprisingly this mass number is that of an acetone dimer. Lateral interactions[17] of adsorbed acetone molecules have been reported previously, and that might be the case here as well.

TABLE 1: Activation Energies of Acetone Desorption from Single-Walled Carbon Nanotubes Calculated from Thermal Desorption Spectrum of the $m/e = 43$ Signal

peak temperature T_{max} °C	E_a kcal mol^{-1}
78	24.5
186	32.3
353	44.5
441	50.9
558	59.5

The activation energy of desorption was calculated from desorption peak temperatures using the Redhead equation.[18−21] It can be seen that the activation energy (Table 1) for desorption of acetone is much larger than the latent heat of vaporization of acetone from the liquid state (7.41 kcal/mol) and activation energy of desorption of acetone multilayer from graphite.[22,9] These values are interesting when compared to the enthalpy of adsorption of acetone on activated carbon (9.32 kcal/mol)[23] and graphitized carbon[24] (7.6 kcal/mol) from the perspective of application of nanotubes in membrane and separation technologies. Chemisorption is further confirmed by the very high activation energy of desorption, which is comparable to that of the covalent bond energy.

Two of the characteristic Raman active modes of single-walled carbon nanotubes are (1) the diameter-dependent radial breathing mode (ω_{RBM}) found around 180 cm^{-1}−260 cm^{-1} and (2) the G band found around 1500−1600 cm^{-1}. The mode at ca. 1320 cm^{-1} represents the disorder or sp^3 character in nanotubes. The G band is a multicomponent spectral feature associated with the tangential displacements of the C−C bond stretching vibrations. The peaks between 1580 and 1590 cm^{-1} can be associated with the lattice C−C stretching vibrations E_2, A, E_1, respectively.[25] Compared to the pristine single-walled nanotubes, the acetone sonicated nanotubes showed a downshift in all the G band modes including the 1591 cm^{-1} peak, which was downshifted by 6 cm^{-1}. It was also observed that the intensity (relative to 1590 cm^{-1}) of the Breit-Wigner-Fano (BWF) line (∼1550 cm^{-1}) decreased. Studies show that their relative intensity is dependent on the intrabundle interactions.[26] Adsorption of acetone, aided by sonication, would lead to a decrease in the intertube interactions. All the G band peaks shifted back to those of the pristine nanotube after TDP and the BWF line intensity was also recovered, but an increase in the intensity ratio of D/G (from 0.12 to 0.25) was found. A similar downshift (4 cm^{-1}) and recovery was seen in the peaks of the radial breathing mode. These changes in Raman modes also suggest some kind of chemical modification of the nanotube surface.

To obtain an atomic level understanding of the interaction between acetone molecule and the nanotube surface we carried out a theoretical study using hybrid quantum mechanical and semiempirical methods. In particular ,we used the two-level ONIOM[27,28] method and Gaussian 98 code.[29] The total system is divided into two levels: a small part of the nanotube and acetone are treated within the density functional approach (high

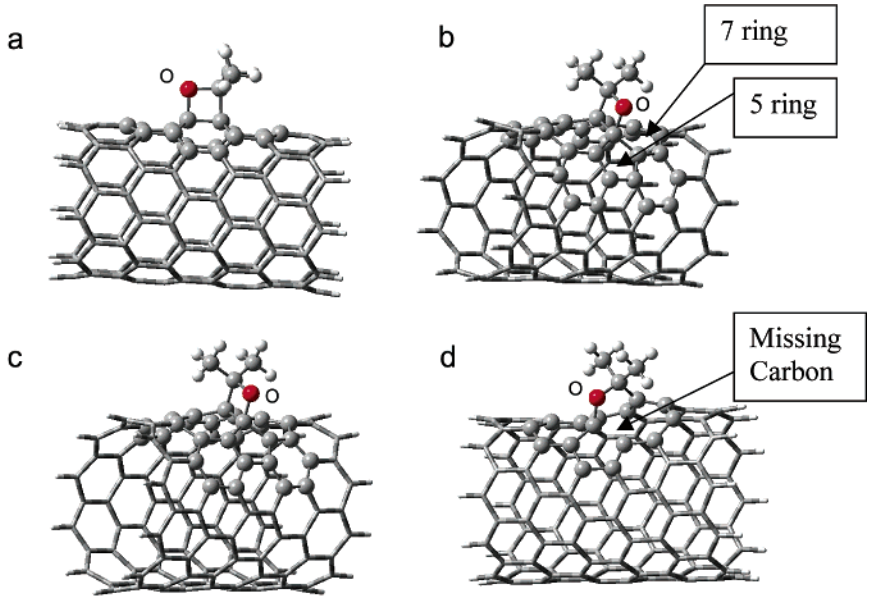

Figure 4. Optimized structures for acetone adsorbing on the surface of (a) perfect (9,0) SWNT, (b) (9,0) SWNT with a Stone-Wales defect, (c) (10,0) SWNT with a Stone-Wales defect and (d) (10,0) SWNT with a vacancy.

level), whereas the remaining part of the system is treated by the semiempirical PM3 method[30,31] (low level). We used the gradient-corrected PW91[32] scheme and 3-21G basis sets for our density functional calculation. The above functional and basis sets are considered to be a good choice for reproducing experimental energetics and bond lengths of nanotubes and their interaction with small molecules.[33] The dangling bonds at both ends of the nanotube are saturated by hydrogen bonds. Besides the perfect nanotube, the interactions of acetone with topological defects such as the Stone-Wales defect[34] and vacancies have been investigated. The binding energy (adsorption energy) of a single acetone molecule on the nanotube is defined as

$$E_{\text{binding}} = E_{\text{nanotube+acetone}} - E_{\text{nanotube}} - E_{\text{acetone}}$$

where $E_{\text{nanotube+acetone}}$, E_{nanotube}, and E_{acetone} are the total energies of the fully relaxed structures of a nanotube containing a single acetone adsorbate, an isolated nanotube, and an isolated acetone molecule, respectively.

First we investigated the possibility of acetone chemisorption on a perfect (9,0) single-walled carbon nanotube (SWNT). Here 28 carbon atoms at the center of the (9,0) tube (total $C_{108}H_{18}$ atom), together with the acetone molecule, are treated using a high-level ONIOM calculation. After geometry optimization using the ONIOM approach, the optimized C−C bond lengths of the $C_{108}H_{18}$ tube range from 1.37 to 1.48 Å, which is in agreement with earlier studies and close to the C−C distance in graphite (1.42 Å). We have considered various sites (such as on-top, between the C−C bonds, center of the hexagonal ring) on the nanotube surface for acetone adsorption, and the lowest energy structure is shown in Figure 4a. Although the above structure corresponds to a local minimum in the total energy calculation ,the binding energy of adsorption (see above for definition) is found to be negative. This suggests that chemisorption of acetone on the perfect nanotube is not thermodynamically preferred.

It is now well-known that defects could be present in nanotubes and they could modify the interactions of the nanotube with adsorbates drastically. We have considered the interaction of acetone with the nanotube in the presence of one of the simplest topological defects known as the Stone-Wales (SW) defect on the nanotube surface. A Stone-Wales defect corresponds to the rotation of one of the bonds in the hexagonal network by 90°, resulting in a double 5−7 defect pair and is observed on the nanotube surface by experiments. As in the case of the perfect nanotube, 28 carbon atoms of SWNT around the defect site and the acetone molecule are treated using a high-level scheme. We have considered various sites of adsorption and the optimized structure of an acetone molecule on a (9,0) nanotube surface in the presence of a SW defect is shown in Figure 4b. The computed binding energy of acetone adsorption is found to be 23.1 kcal/mol, which can be compared to the desorption energy of 24.5 kcal/mol obtained using a temperature-programmed desorption (TPD) experiment. Since, in experiments, nanotubes with different diameters in the range of 0.9−1.34 nm are present, we have also considered the interaction of acetone with a (10,0) SWNT in order to study the variation of binding energy as a function of diameter. Figure 4c shows the optimized structure of an acetone molecule on a (10,0) SWNT in the presence of a SW defect. The computed binding energy in this case is 16.1 kcal/mol, which suggests that the different peaks in the TPD experiment shown earlier could be due to the interaction of acetone with nanotubes of different diameters. It is quite possible that the different binding energy values obtained in experiment could also be due to other similar defects present in the system. However, the peak in the TPD at about 558 K corresponding to 59.5 kcal/mol binding energy suggests that defects completely different in nature may account for this large adsorption energy. The interaction of acetone in the presence of a vacancy on the nanotube surface has been considered and Figure 4d shows the chemisorption of acetone on a (10,0) SWNT. Fifteen carbon atoms around the defect site and the acetone molecule are treated using a high-level scheme in the ONIOM method. The acetone is adsorbed on a bridge site of two dangling carbon atoms. The C═O double bond of the acetone molecule is weakened into a single bond. The computed binding energy of 59.0 kcal/mol can be compared with the peak at higher temperature in the TPD experiment corresponding to 59.5 kcal/mol desorption energy. This excellent agreement between theory and experiment is certainly a coincidence, but it clearly suggests that the bonding between acetone and the

nanotube becomes stronger due to the existence of a defect. Here we have considered a few types of topological defects as examples of the role of defects in chemisorption of acetone. Of course, there could be many other types of defects such as sp^3 carbon defects, vacancy saturated with hydrogen defects, etc., which we have not considered in our calculation but could account for other desorption peaks. We should also mention here that our calculations were carried out by considering an isolated single-walled nanotube, while experiments were performed on nanotube bundles; quantitative comparison between the theory and experiment should be done with caution.

4. Conclusions

In summary, we have studied the interaction of acetone on carbon nanotubes using temperature-programmed desorption, X-ray photoelectron spectroscopy, and Raman spectroscopy. All these techniques indicate that the chemisorption of acetone occurs on carbon nanotubes, thereby changing the surface character of the tubes. The energy of adsorption of acetone on nanotubes was found to be higher than that of graphite and activated carbon. The interaction of acetone on the nanotube surface was studied theoretically using hybrid quantum mechanical and semiempirical methods. We find that the defects are essential for acetone to bind chemically on the nanotube surface. The binding energy also depends on the diameter of the nanotube. The present theoretical study suggests that the binding energy dependence on diameter could be nonmonotonic in nature. Activated carbon black is used for removal of organic pollutants including acetone from industrial wastes. Carbon nanotubes, with their very high surface areas, are better candidates. The strong (and possibly selective) interaction of solvents such as acetone with nanotubes suggests possible application of nanotube membranes in solvent separation. The electronic properties and hence the transport characteristics of nanotubes will change with adsorbed molecules. It becomes all the more clear from our study that defect-free nanotubes are essential for achieving the predicted electronic properties for nanotubes. But this has not been achieved for nanotubes available today since they seem to have defects, a fact that is evident from our experimental studies and supporting calculations on acetone adsorption on nanotubes.

Acknowledgment. The authors from the Materials Science Department thank Professor G. Ramanath (RPI) and Rory Leahy (RPI) for running the thermal desorption spectra and the Clemson Grant (NSF award number DMR-0070661) for funding the project. This work was also partly supported (N.C., P.M.A., Y.M.Z., and S.K.N.) by the NSF-funded Nanoscale Science and Engineering Center (NSEC) at RPI and by (Y.M.Z. and S.K.N.) National Computational Science Alliance under Grant MCA01S-014N.

References and Notes

(1) Hilding, J.; Grulke, E. A.; Sinnott, S. B.; Qian, D.; Andrews, Z.; Jagtoyen, M. *Langmuir* **2001**, *17*, 7540.

(2) Teizer, W.; Hallock, R. B.; Dujardin, E.; Ebbesen, T. W. *Phys. Rev. Lett.* **1999**, *82*, 5305.

(3) Muris, M.; Dufau, N.; Bienfait, N.; Dupont-Pavlovsky, N.; Grillet, Y., Palmari, J. P. *Langmuir* **2000**, *16*, 7019.

(4) Talapatra, S.; Zambano, A. Z.; Weber, S. E.; Migone, A. D. *Phys. Rev. Lett.* **2000**, *85*, 138.

(5) Kuznetsova, A.; Yates, J. T.; Liu, J.; Smalley, R. E. *J. Chem. Phys.* **2000**, *112* (21), 9590.

(6) Long, R. Q.; Yang, R. T. *J. Am. Chem. Soc.* **2001**, *123*, 2058.

(7) Koshio, A.; Yudasaka, M.; Zhang, M.; Iijima, S. *Nano Lett.* **2001**, *7*, 361.

(8) Sun, Y.; Wilson, S. R.; Schuster, D. I. *J. Am. Chem. Soc.* **2001**, *123*, 5348.

(9) Kwon, S.; Russell, J.; Zhao, X.; Vidic, R. D.; Johnson, J. K.; Borguet, E. *Langmuir* **2002**, *18*, 2595.

(10) Dinger, A.; Lutterloh, C.; Biener, J.; Kueppers, J. *Surf. Sci.* **1999**, *437*, 116.

(11) Muris, M.; Dupont-Pavlovsky, N.; Bienfait, M.; Zeppenfeld, P. *Surf. Sci.* **2001**, *492*, 67.

(12) Thomy, A.; Duval, X. *Surf. Sci.* **1994**, *299*−*300*, 415.

(13) Nikolaev, P.; Bronikowski, M. J.; Bradley, R. K.; Rohmund, F.; Colbert, D. T.; Smith, K. A.; Smalley, R. E. *Chem. Phys. Lett.* **1999**, *313*, 91.

(14) Armstrong, J. L.; White, J. M.; Langell, M. *J. Vac. Sci. Technol. A* **1997**, *15*, 3.

(15) *Eight-Peak Index of Mass Spectra*; Mass Spactrometry Data Centre: Nottingham, 1986.

(16) Cho, S.; Chung, C.; Moon, S. H. *Thin Solid Films* **2002**, *98*, 104.

(17) Parcher, J. F.; Hyver, K. J.; Johnson, D. M.; Ping, D. M.; Lin, J. *J. Chromatogr.* **1985**, *328*, 63.

(18) Redhead, P. A. *Vacuum* **1962**, *12*, 203.

(19) de Jong, A. M.; Niemantsverdriet, J. W. *Surf. Sci.* **1990**, *233*, 355.

(20) Sakakini, B. H.; Verbrugge, A. S. *J. Chem. Soc., Faraday Trans.* **1997**, *93* (8), 1637−1640.

(21) $E_a = RT_{max}[\ln(AT_{max}/\beta) - 3.64]$, the Redhead equation, is derived from the relation $E_a/RT_{max}^2 = [A/\beta]\exp(-E_a/RT_{max})$; here, R is the universal gas constant, T_{max} is the peak temperature, A is the preexponential factor of desorption, and β (in this cae, 0.05 K/s) is the heating rate. The preexponential factor was assumed to be 10^{13}, which is the case for coverage-independent desorption. The relation between E_a and T_{max} is very nearly linear and can be taken as a constant. This equation is often used to determine E_a from a single desorption spectrum.

(22) Cox, J. D.; Pilcher, G. *Thermochemistry of Organic and Organometallic Compounds*; Academic Press: New York, 1970.

(23) Gales, L.; Mendes, A.; Costa, C. *Carbon* **2000**, *38*, 1088.

(24) Elkington, P. A.; Curthots, G. *J. Phys. Chem.* **1969**, *73*, 2321.

(25) Kukovecz, A.; Kramberger, C.; Georgakilas, V.; Prato, M.; Kuzmany, H. *Eur. Phy. J., B* **2002**, *28*, 223.

(26) Jiang, C.; Kempa, K.; Zhao, J.; Schlecht, U.; Kolb, U.; Basche, T.; Burghard, M.; Mews, A. *Phys. Rev. B* **2002**, *66*, 161404.

(27) Svensson, M.; Humbel, S.; Froese, R. D. J.; Matsubara, T.; Sieber, S.; Morokuma, K. *J. Phys. Chem.* **1996**, *100*, 19357.

(28) Dapprich, S.; Komaromi, I.; Byun, K. S.; Morokuma, K.; Frisch, M. J. *J. Mol. Struct. (Theochem)* **1999**, *1*−*2*, 461.

(29) Frisch, M. J.; et al. *Gaussian 98* (Revision A.9); Gaussian, Inc.: Pittsburgh, PA, 2001.

(30) Stewart, J. J. P. *J. Comput. Chem*. **1989**, *10*, 209.

(31) Stewart, J. J. P. *J. Comput. Chem*. **1989**, *10*, 221.

(32) Perdew, J. P.; Burke, K.; Wang, Y. *Phys. Rev. B* **1996**, *54*, 16533.

(33) Bettinger, H. F.; Kudin, K. N.; Scuseria, G. E. *J. Am. Chem. Soc.* **2001**, *123*, 12849.

(34) Stone, A. J.; Wales, D. J. *Chem. Phys. Lett.* **1986**, *128*, 501.